Geotech Geol Eng (2019) 37:3781–3804
https://doi.org/10.1007/s10706-019-00868-3

ORIGINAL PAPER

Shock Reduction Techniques for a Submarine Tunnel

Xuansheng Cheng · Taifeng Kang · Caiquan Yue · Xiuli Du

Received: 22 December 2018 / Accepted: 19 March 2019 / Published online: 25 March 2019

Abstract Considering the effects of seepage and dynamic pressure, defining a rock mass as a saturated porous media, and using the finite element method, a dynamic fluid–structure interaction model of a subsea tunnel with a viscous spring artificial boundary is established. Adopting rubber and foam concrete as shock absorption layers and inputting both horizontal and vertical earthquake waves, the time history curves of the first principal stress at key points in the secondary lining structure are comparatively analyzed based on the presence and absence of shock absorption layers. The principal stress peaks are also analyzed. The damping effect of the shock absorption layer is studied. The results show that the peak and principal stresses at the main parts of the tunnel lining structure decrease after the shock absorption layer is established. Obvious decreases occur in the vault and inverted arch. A certain degree of peak stress reduction is also observed after the shock absorption layer is established. Establishing the shock absorption layer does not change the spectrum characteristics of the tunnel structure. Foam concrete shock absorption is recommended because the damping effect of foam concrete is more observable than that of rubber.

Keywords Seepage · Earthquake · Submarine tunnel · Rubber · Foam concrete · Shock reduction

X. Cheng (✉) · T. Kang · C. Yue
School of Civil Engineering, Lanzhou University of Technology, Lanzhou 730050, People's Republic of China
e-mail: chengxuansheng@gmail.com

X. Cheng · X. Du
Key Laboratory of Urban Security and Disaster Engineering of Education, Beijing University of Technology, Beijing 100124, People's Republic of China

1 Introduction

With the rapid development of the economy and engineering technology, underground space development has recently received considerable attention. Underground structures such as subways, cross-river tunnels, and undersea tunnels have gradually increased. Specifically, undersea tunnels are highly convenient for travel and promote the development of regional economies. These tunnels can link various islands and landmasses, prompting numerous countries to develop such infrastructures. However, constructing and maintaining submarine tunnels is very difficult because of the complexities presented by the geological and marine environments. The prevention of water infiltration and submarine tunnel seismic activity are major technical problems. "Water and Tunnels" was the theme of the 1988 Madrid International Conference held by the International Tunneling Association. Since then, numerous scholars have studied waterproof engineering for submarine tunnel structures. Severe water seepage occurred twice in the Seikan Submarine Tunnel, which was constructed in 1964 in Japan. The incidents not only caused considerable casualties and property losses but also impeded tunnel construction. Given this background, an important practical requirement is the investigation of shock absorption technology in submarine tunnels, in which the roles of fluid–structure interactions (FSI) and seepage are examined.

Research on shock absorption in tunnel structures began with shield tunnels. Japanese scholar Suzuki Meng Kang's study was based on establishing a shock absorption layer between the rock mass and submarine tunnel lining. Through this process, the binding of the rock mass surrounding the tunnel is cut off, and the strain and relative displacement between the tunnel structure and the rock mass surrounding the tunnel are absorbed by the shock absorption layer.

Seismic responses cannot be obtained when a tunnel structure is separated from the site soil. Thus, reducing earthquake actions by extending the structure period is infeasible. Isolation support or other damping devices cannot be installed because the tunnel structure is covered under the site soil. Two approaches to shock absorption are currently employed (Liu et al. 2010). The first approach changes the performance of the tunnel to mitigate the internal force of the tunnel lining. The second approach establishes a shock absorption layer or grouting consolidation layer between the tunnel lining and rock/soil mass that prohibits ground deformation from extending to the tunnel lining. Wang et al. (1996) discussed the feasibility of the concept at the technical level and proposed an underground structure shock absorption model based on an investigation of a tunnel entrance from the perspective of shock absorption. The model test and numerical analysis results were based on the principle of structural damping associated with a ground structure. Wang and Cui (2010) established a damping model with a shock absorption layer in a tunnel support system and explored the damping influence of the seismic wave input frequency, shock absorption layer damper, and stiffness. Huang et al. (2009) simulated the damping effect of a rubber-and-foam concrete shock absorption layer using ABAQUS software. Xiong et al. (2007) studied the seismic response of the Huangcaoping tunnel using a numerical simulation and explored the effects of the shock absorption layer and seismic joint on the surrounding rock, lining stress, acceleration, and displacement. Gao and Chen (2008) analyzed the applicable conditions of two damping measures in the construction of soft rock/soil tunnels. Yuan (2008) discussed the seismic response of the lining structure to the lining thickness, lining material stiffness, burial depth, and other similar factors in shallow tunnels. Gao (2001) analyzed the seismic responses of long tunnels in high-intensity seismic regions and studied the tunnel damping effect by establishing a shock absorption layer and seismic joint. Wang (2008) simulated the seismic dynamic response of the entrance section of a double-arch tunnel and summarized the dynamic response trends based on several parameters, such as the middle wall thickness, rock/soil parameters, and seismic intensity. The shock absorption effect on the establishment of shock absorption layers and seismic joints was also investigated. Kim and Konagai (2000) studied the seismic isolation effect of a tunnel covered with a coating material.

Using FLAC3D software, Li (2006) analyzed the seismic response and damping measures of a mountain tunnel under various conditions. Sun (2009) established several models of a tunnel located in a high-intensity zone and discussed and analyzed the seismic absorption effects of vibration absorption and resistance measures using ABAQUS software. Gao et al. (2005) studied the response of a tunnel using Newmark's step-by-step implicit integration finite element method and a viscous spring artificial boundary technique under various earthquake accelerations and soil mass multiform conditions. Ling and Gao (2008) studied the damping effect of grouting consolidation and the shock absorption cushion under the same earthquake action using a soil–structure interaction model and a time-dependent analysis method. Hasheminejad and Miri (2008) examined the seismic isolation effect on lined circular tunnels with damping treatments. Kim and Konagai (2000) and Konagai and Kim (2001) studied the damping effect by adding a flexible material into the cover layer of a tunnel. Shimamura et al. (1999) investigated the seismic isolation effect in a rectangular-shaped tunnel with a soft isolation layer. Cheng et al. (2013) defined the rock mass surrounding a tunnel as a continuous porous medium and studied a subsea tunnel passing through a broken zone. The results showed that the hydrodynamic pressure in the porous rock medium had significant effects on the structural internal force of the tunnel. Additionally, the stresses and strains at the spandrel and both sides of the tunnel lining dramatically increased under seismic action. For a lightly weathered rock mass, Cheng et al. (2016, 2017a, b) studied the seismic stability of a cross-sea tunnel with and without shock absorption under seepage and bi-directional earthquake conditions. The study found that the sea depth and permeability coefficient had little effect on the safety factor.

As indicated above, research on the seismic isolation of tunnels has primarily centered on onshore tunnels, whereas studies of damping measures in submarine tunnels with consideration of seepage are relatively scarce. Cheng et al. (2014a, b, 2017a, b, 2018) studied the seismic stability of subsea tunnels subjected to seepage and the seismic response of fluid–structure interactions in undersea tunnels during earthquakes or sea wave. Thus, a research base has been provided for shock absorption technology associated with tunnels under seepage actions. In this study, dynamic finite element analysis software is used to establish a two-dimensional fluid–structure coupled model of a submarine tunnel. We assume that a tunnel with a shock absorption layer has been built. The tunnel rock mass is defined as the equivalent porous medium. Considering bidirectional earthquake actions and FSIs between the pore water and saturated rock mass in saturated fractured zones and using foam concrete and rubber materials as a damping layer, the damping effect is comparatively studied. The results of this research can serve as framework for the design of damping measures for submarine tunnels.

2 Dynamic Finite Element Analysis

2.1 Dynamic Analysis Equation

According to Biot's dynamic consolidation theory (Xie and Zhou, 2002), disregarding the compressibility of the pore fluid, the saturated pore fluid continuity equation is as follows:

$$\frac{\partial \varepsilon_{ii}}{\partial t} + \frac{1}{\gamma_f} \nabla^T(-\boldsymbol{K}(\nabla P)) = 0, \tag{1}$$

where $\bigtriangledown$ is the Laplace operator, $\boldsymbol{K}$ is the permeability coefficient matrix of the rock/soil mass, ε_{ii} is the volume strain of the rock/soil mass skeleton, P is the pore water pressure, and γ_f is the unit weight of the pore fluid.

When the relative acceleration of the pore fluid in the rock/soil mass and geotechnical compressibility are disregarded, the dynamic equilibrium equation of the saturated rock/soil mass is as follows:

$$\sigma'_{ij,i} + p_{,j}\delta_{ij} + \rho b_i = \rho \ddot{u}_i \, (i,j = 1,2,3),, \tag{2}$$

where $\sigma'_{ij,i}$ is the effective stress, δ_{ij} is the Kronecker delta, ρ is the density of the rock/soil mass, b_i represents the volume force acceleration, and $\ddot{u}_i$ denotes the acceleration of the rock/soil mass skeleton.

According to elastic dynamics theory, the dynamic control equation of the subsea tunnel lining structure is as follows:

$$\sigma_{pij,j} + \rho_p b_{pi} = \rho_p \ddot{u}_{pi} \, (i,j = 1,2,3),, \tag{3}$$

where σ_{pij}, ρ_p, b_{pi}, and $\ddot{u}_{pi}$ are the internal stress, mass density, volume force acceleration, and acceleration of the subsea tunnel lining structure, respectively.

2.2 Dynamic Finite Element Equation and Numerical Solution Method for Saturated Rock/Soil Mass and a Subsea Tunnel Lining Structure

1. Dynamic finite element equation of the saturated rock/soil mass

The Galerkin method is used in this study (Wang and Dong, 2003). According to the finite element discretization of Eqs. (1) and (2), the FSI dynamic finite element equation of the saturated rock/soil mass is derived as follows.

$$\begin{bmatrix} {}^{t+\Delta t}\boldsymbol{M} & 0 \\ 0 & 0 \end{bmatrix} \begin{Bmatrix} {}^{t+\Delta t}\ddot{\boldsymbol{U}} \\ {}^{t+\Delta t}f \end{Bmatrix} + \begin{bmatrix} {}^{t+\Delta t}(\boldsymbol{C}+\boldsymbol{C}') & 0 \\ {}^{t+\Delta t}\boldsymbol{K}^T_{up_f} & 0 \end{bmatrix} \begin{Bmatrix} {}^{t+\Delta t}\dot{\boldsymbol{U}} \\ {}^{t+\Delta t}\dot{\boldsymbol{p}}_f \end{Bmatrix} + \begin{bmatrix} {}^{t+\Delta t}\boldsymbol{K}_{uu} & {}^{t+\Delta t}\boldsymbol{K}_{up_f} \\ 0 & -{}^{t+\Delta t}\boldsymbol{K}_{p_f p_f} \end{bmatrix} \begin{Bmatrix} {}^{t+\Delta t}\boldsymbol{U} \\ {}^{t+\Delta t}\boldsymbol{p}_f \end{Bmatrix} = \begin{Bmatrix} {}^{t+\Delta t}\boldsymbol{R}_u \\ {}^{t+\Delta t}\boldsymbol{R}_{p_f} \end{Bmatrix} \tag{4}$$

$$ {}^{t+\Delta t}\boldsymbol{K}_{uu} = \sum_m \int_{t+\Delta t_{v}(m)} {}^{t+\Delta t}\boldsymbol{B}_u^{(m)^T}\, {}^{t+\Delta t}\boldsymbol{D}^{(m)}\, {}^{t+\Delta t}\boldsymbol{B}_u^{(m)}\, d^{t+\Delta t}v^{(m)} \tag{5a} $$

$$ {}^{t+\Delta t}\boldsymbol{K}_{up_f} = \sum_m \int_{t+\Delta t_{v}(m)} {}^{t+\Delta t}\boldsymbol{B}_u^{(m)^T}\, \boldsymbol{I}^{(m)}\, {}^{t+\Delta t}\boldsymbol{H}_{p_f}^{(m)}\, d^{t+\Delta t}v^{(m)} \tag{5b} $$

$$ {}^{t+\Delta t}\boldsymbol{K}_{p_f p_f} = \frac{1}{\gamma_f}\sum_m \int_{t+\Delta t_{v}(m)} {}^{t+\Delta t}\boldsymbol{B}_{p_f}^{(m)^T}\, {}^{t+\Delta t}\boldsymbol{K}^{(m)}\, {}^{t+\Delta t}\boldsymbol{B}_{p_f}^{(m)}\, d^{t+\Delta t}v^{(m)} \tag{5c} $$

$$ {}^{t+\Delta t}\boldsymbol{R}_{p_f} = \sum_m \int_{t+\Delta t_{s_q^{(m)}}} \left({}^{t+\Delta t}\boldsymbol{H}_{p_f}^{{}^{t+\Delta t}s_q^{(m)}(m)}\right)^T {}^{t+\Delta t}\boldsymbol{q}^{(m)}\, d^{t+\Delta t}s_q^{(m)} \tag{5d} $$

$$ {}^{t+\Delta t}\boldsymbol{R}_u = \sum_m \int_{t+\Delta t_{v^{(m)}}} {}^{t+\Delta t}\boldsymbol{H}_u^{(m)^T}\, {}^{t+\Delta t}\boldsymbol{f}^{(m)}\, d^{t+\Delta t}v^{(m)} + \sum_m \int_{t+\Delta t_{s_f^{(m)}}} \left({}^{t+\Delta t}\boldsymbol{H}_u^{{}^{t+\Delta t}s_f^{(m)}(m)}\right)^T {}^{t+\Delta t}\boldsymbol{f}^{(m)}\, d^{t+\Delta t}s_f^{(m)} \tag{5e} $$

In Eqs. (4)–(5), $\boldsymbol{U}$ and $\boldsymbol{P}_{\mathrm{f}}$ are the geotechnical nodal displacement and pore water pressure vectors, respectively; $\boldsymbol{M}$ and $\boldsymbol{C}$ denote the rock/soil mass and damping matrices, respectively; $\boldsymbol{C}'$ is the damping caused by shock absorption; $\boldsymbol{D}$ is the geotechnical flexibility coefficient matrix; $\boldsymbol{f}$ and $\boldsymbol{q}$ are load vectors; $\boldsymbol{B}_u$ and $\boldsymbol{B}_{pf}$ represent the nodal displacement and pore water pressure of the rock/soil mass geometry gradient matrix, respectively; $\boldsymbol{H}_{\mathrm{u}}$ and $\boldsymbol{H}_{\mathrm{pf}}$ are the interpolation function matrices of the nodal displacement and pore water pressure of the rock/soil mass, respectively; and $\boldsymbol{I}$ is the unit matrix.

2. Dynamic finite element equation of the tunnel lining structure

Here, the Galerkin method is also applied. According to the finite element discretization in Eq. (3), the dynamic finite element equation of the tunnel lining structure can be obtained as follows.

$$ {}^{t+\Delta t}\boldsymbol{M}_p\, {}^{t+\Delta t}\boldsymbol{\mathcal{U}}_p + {}^{t+\Delta t}\left(\boldsymbol{C}_p + \boldsymbol{C}'_p\right) {}^{t+\Delta t}\dot{\boldsymbol{U}}_p + {}^{t+\Delta t}\boldsymbol{K}_{\mathrm{uup}}\, {}^{t+\Delta t}\boldsymbol{U}_p = {}^{t+\Delta t}\boldsymbol{R}_{\mathrm{up}} \tag{6} $$

$$ {}^{t+\Delta t}\boldsymbol{K}_{uup} = \sum_m \int_{t+\Delta t_{v_p^{(m)}}} {}^{t+\Delta t}\boldsymbol{B}_{up}^{(m)^T}\, {}^{t+\Delta t}\boldsymbol{D}_p^{(m)}\, {}^{t+\Delta t}\boldsymbol{B}_{up}^{(m)}\, d^{t+\Delta t}v_p^{(m)} \tag{7a} $$

$$ {}^{t+\Delta t}\boldsymbol{R}_{up} = \sum_m \int_{t+\Delta t_{v_p^{(m)}}} {}^{t+\Delta t}\boldsymbol{H}_{up}^{(m)^T}\, {}^{t+\Delta t}\boldsymbol{f}_p^{(m)}\, d^{t+\Delta t}v_p^{(m)} + \sum_m \int_{t+\Delta t_{s_{f_p}^{(m)}}} \left({}^{t+\Delta t}\boldsymbol{H}_{up}^{{}^{t+\Delta t}s_f^{(m)}(m)}\right)^T {}^{t+\Delta t}\boldsymbol{f}_p^{(m)}\, d^{t+\Delta t}s_{f_p}^{(m)} \tag{7b} $$

In Eqs. (6)–(7), $\boldsymbol{U}_p$ is the nodal displacement vector; $\boldsymbol{M}_p$ and $\boldsymbol{C}_p$ are the mass and damping matrices, respectively; $\boldsymbol{C}'_p$ is the damping caused by shock absorption; $\boldsymbol{D}_p$ is the elasticity coefficient matrix; $\boldsymbol{f}_p$ denotes the load vector; $\boldsymbol{B}_{up}$ represents the geometry gradient matrix of the nodal displacement; and $\boldsymbol{H}_{up}$ is the interpolation function matrix of the nodal displacement.

3. Dynamic finite element equation and numerical solution method of the saturated rock/soil mass of the undersea tunnel lining structure

To simultaneously solve Eqs. (4) and (6), the Newmark-β is used.

$$ \begin{cases} \begin{bmatrix} {}^{t+\Delta t}\boldsymbol{K}_{uu} + \alpha_0 {}^{t+\Delta t}\boldsymbol{M} + \alpha_1 {}^{t+\Delta t}\boldsymbol{C} & {}^{t+\Delta t}\boldsymbol{K}_{up_f} \\ \boldsymbol{K}_{up_f}^T & -\Delta t^{t+\Delta t}\boldsymbol{K}_{p_f p_f} \end{bmatrix} \begin{Bmatrix} {}^{t+\Delta t}\boldsymbol{U} \\ {}^{t+\Delta t}\boldsymbol{P}_f \end{Bmatrix} \\ = \begin{Bmatrix} {}^{t+\Delta t}\boldsymbol{R}_u^d \\ -\Delta t^{t+\Delta t}\boldsymbol{R}_{p_f} + {}^{t+\Delta t}\boldsymbol{K}_{up_f}^T\, {}^t\boldsymbol{U} \end{Bmatrix} ({}^{t+\Delta t}\boldsymbol{K}_{\mathrm{uup}} + \alpha_0 {}^{t+\Delta t}\boldsymbol{M}_{\mathrm{p}} + \alpha_1 {}^{t+\Delta t}\boldsymbol{C}_{\mathrm{p}})^{t+\Delta t}\boldsymbol{U}_p = {}^{t+\Delta t}\boldsymbol{R}_{up}^d \end{cases} \tag{8} $$

$$ {}^{t+\Delta t}\boldsymbol{R}_u^d = {}^{t+\Delta t}\boldsymbol{R}_u + {}^{t+\Delta t}\boldsymbol{M}(\alpha_0 {}^t\boldsymbol{U} + \alpha_2 {}^t\dot{\boldsymbol{U}} + \alpha_3 {}^t\ddot{\boldsymbol{U}}) + {}^{t+\Delta t}\boldsymbol{C}(\alpha_1 {}^t\boldsymbol{U} + \alpha_4 {}^t\dot{\boldsymbol{U}} + \alpha_5 {}^t\ddot{\boldsymbol{U}}) \tag{9a} $$

$$ {}^{t+\Delta t}\boldsymbol{R}_{up}^d = {}^{t+\Delta t}\boldsymbol{R}_{up} + {}^{t+\Delta t}\boldsymbol{M}_p(\alpha_0 {}^t\boldsymbol{U}_p + \alpha_2 {}^t\dot{\boldsymbol{U}}_p + \alpha_3 {}^t\ddot{\boldsymbol{U}}_p) + {}^{t+\Delta t}\boldsymbol{C}_p(\alpha_1 {}^t\boldsymbol{U}_p + \alpha_4 {}^t\dot{\boldsymbol{U}}_p + \alpha_5 {}^t\ddot{\boldsymbol{U}}_p) \tag{9b} $$

In Eqs. (8)–(9), $\alpha_0 = \frac{1}{\alpha\Delta t^2}$, $\alpha_1 = \frac{\beta}{\alpha\Delta t}$, $\alpha_2 = \frac{1}{\alpha\Delta t}$, $\alpha_3 = \frac{1}{2\alpha} - 1$, $\alpha_4 = \frac{\beta}{\alpha} - 1$, and $\alpha_5 = \Delta t(\frac{\beta}{2\alpha} - 1)$. Generally, when $\beta \geq 0.5$ and $\alpha \geq 0.25(0.5+\beta)^2$, the Newmark-$\beta$ method is unconditionally stable. In this study, we set $\alpha = 0.8$ and $\beta = 0.6$.

2.3 Governing Equations of Seawater

Assuming that the wave is one dimensional and has a small linear amplitude and that the water depth is H, the control equations and boundary conditions that the potential function (x, y, z, t) satisfies are as follows.

$$\nabla^2 \Phi = 0, \quad -H < z < 0 \tag{10}$$

$$\frac{\partial \Phi}{\partial z} - \frac{\partial \eta}{\partial t} = 0, \quad z = 0 \tag{11}$$

$$\frac{\partial \Phi}{\partial z} + g\eta = 0, \quad z = 0 \tag{12}$$

$$\frac{\partial \Phi}{\partial z} = 0, \quad z = -H \tag{13}$$

Combining Eqs. (11) and (12) and eliminating η yields Eq. (14).

$$\frac{\partial^2 \Phi}{\partial t^2} + g\frac{\partial \Phi}{\partial z} = 0, \quad z = 0 \tag{14}$$

Assuming that the free surface of the wave is a simple harmonic wave form, the following relationship holds (Tao 2005):

$$\eta(x,t) = ae^{ikx}e^{-i\omega t} \tag{15}$$

$$\Phi(y,z,t) = \phi(y,z)e^{-i\omega t}, \tag{16}$$

where a is the amplitude and k is the wavenumber.

Substituting Eqs. (15) and (16) into Eqs. (10)–(14), conditions ϕ and η can be obtained.

$$\nabla^2 \phi = 0, \quad -H < z < 0 \tag{17}$$

$$\frac{\partial \phi}{\partial z} = 0, \quad z = -H \tag{18}$$

$$\frac{\partial \phi}{\partial z} + i\omega ae^{iky} = 0, \quad z = 0 \tag{19}$$

$$gae^{iky} - i\omega\phi = 0, \quad z = 0 \tag{20}$$

According to Eqs. (19) and (20), the following expression can be established.

$$\frac{\partial \phi}{\partial z} - \frac{\omega^2}{g}\phi = 0 \tag{21}$$

The potential function ϕ satisfies Eqs. (17) and (18), and ϕ can be expressed as follows (Tao 2005):

$$\phi = A\cosh k(z+H)e^{ikx} \tag{22}$$

where A is a coefficient.

Substituting Eq. (22) into Eq. (20), A can be obtained as follows.

$$A = -\frac{iga}{\omega}\frac{1}{\cosh kH} \tag{23}$$

The potential function corresponding to the small-amplitude problem is obtained as follows.

$$\phi = -\frac{iga}{\omega}\frac{\cosh k(z+H)}{\cosh kH}e^{iky} \tag{24}$$

Substituting the wave height $h = 2a$ and Eq. (24) into Eq. (16) yields the following expression.

$$\Phi(y,z,t) = \frac{gh}{2\omega}\frac{\cosh k(z+H)}{\cosh kH}\sin(ky - \omega t) \tag{25}$$

The wave equation is then given as follows.

$$\eta = \frac{h}{2}\cos(ky - \omega t) \tag{26}$$

2.4 Calculation Process

In calculating the deformation of the rock mass with groundwater, the influence of the pore water pressure on the rock stress and deformation should be considered. After a tunnel is built, the pressure of the rock/soil mass surrounding the tunnel and pore water pressure stabilize the tunnel lining. At this moment, excess pore pressure no longer exists in the rock gaps. To simulate the authenticity of the results, the consolidation degree is first calculated. The completion of consolidation settlement in undersea rock is simulated, and the pore pressure of the rock is eliminated. Restarting the calculation on this basis, the dynamic calculation is continued by adding a seismic load. The calculation process proceeds in the following order: calculation of consolidation settlement → changing of the boundary conditions → imposing a seismic load → restarting the dynamic calculation.

3 Damping Scheme

Tunnel structures are damped by three methods. The first method is to change the performance of the tunnel itself (e.g., stiffness, mass, intensity, and damping) to control the structural stiffness and mass ratios, thereby reducing the internal force on the lining structure. The second method is to establish a damping layer between the tunnel lining and rock/soil mass (mainly, lightweight, soft, and energy-absorbing material with a high damping ratio). In this approach, the lining structure is separated from the rock/soil mass surrounding the tunnel. Transferring the deformation of the rock/soil mass into the tunnel lining is difficult. Thus, the seismic response of the tunnel decreases. The third method is that the rock/soil mass is reinforced by anchor rod grouting, which extends the range of shock absorption.

This study investigates the effect of the second method on shock absorption. The damping layer absorbs dynamic strain. Therefore, the damping layer material must have a certain degree of flexibility to avoid plasticization during an earthquake. This flexibility allows the material to function during the next earthquake. Additionally, considering surface subsidence after construction, the Poisson's ratio value of the damping material should be close to 0.5, or the materials should have a certain anisotropic rigidity in the radial tunnel direction. By setting foam concrete or rubber material between the first and second linings as the shock absorption layer, the history of the first principal stress–time curve and the principal stress peak values at key points in the secondary lining structure can be comparatively analyzed. The different shock absorption effects in the shock absorption layer are examined.

4 Numerical Examples

4.1 Calculation Model

As is shown in Fig. 1, the span and height of the tunnel are assumed to be 15 and 11.25 m, respectively. The cover rock thickness and seawater depth are assumed to be 25 and 10 m, respectively. Considering the scope of influence of the stability of the rock mass surrounding the tunnel, an isolated body with a thickness of 1 m (along the tunnel length) is removed from the semi-infinite space. The calculation ranges are five times the cavern height from the bottom of the tunnel (i.e., 56.25 m) and five times the spans on the left and right sides of the tunnel (i.e., 75 m). A shock absorption layer (0.2 m) is installed between the primary and secondary lining structures. To transmit a seismic wave, a joint constraint boundary is adopted at the bottom of model. Given that water activity is minimal when the seabed depth exceeds a certain value, the interface between the rock mass and seawater below 48 m is a permeable layer, and the remaining portion is an impermeable layer. Porous media are used in the simulation. Considering the effect of sea wave motion, the seawater surface is set as a free surface. Considering the earthquake action, a hydrodynamic pressure is established at the seabed surface. The contact surface between seawater and the cover rock defines the FSI boundary. Considering the absorption capacity of the viscous spring artificial boundary of waves, the rock mass displacement boundary is set as the viscous-spring artificial boundary as follows:

$$K_{BN} = \alpha_N \frac{G}{R}, \quad C_{BN} = \rho c_p \tag{27}$$

$$K_{BT} = \alpha_T \frac{G}{R}, \quad C_{BN} = \rho c_p, \tag{28}$$

where K_{BN} and K_{BT} are the normal and tangential spring stiffnesses, respectively; C_{BN} and C_{BT} are the normal and tangential damping coefficients, respectively; G denotes the shear modulus of the medium; R represents the wave source at the artificial boundary point distance; ρ is the mass density of the medium; and α_N and α_T are the normal and tangential viscous spring boundary correction factors, respectively, which usually range from α_T= 0.35 to 0.65 and α_N = 0.8 to 1.2. In this study, α_T= 0.5 and α_N= 1.0. C_p and C_p are the medium P- and S-wave velocities, respectively:

$$c_p = \sqrt{\frac{\lambda + 2\mu}{\rho}} \tag{29}$$

$$c_s = \sqrt{\frac{\mu}{\rho}}, \tag{30}$$

where λ and μ are the first and second lame parameters, respectively. $\lambda = \frac{\upsilon E}{(1+\upsilon)(1-2\upsilon)}$, and $\mu = \frac{E}{2(1+\upsilon)}$. E and υ are the elastic modulus and Poisson's ratio, respectively. Relevant parameters are assigned values as follows: K_{BN}= 20,242,105 N.s/m,

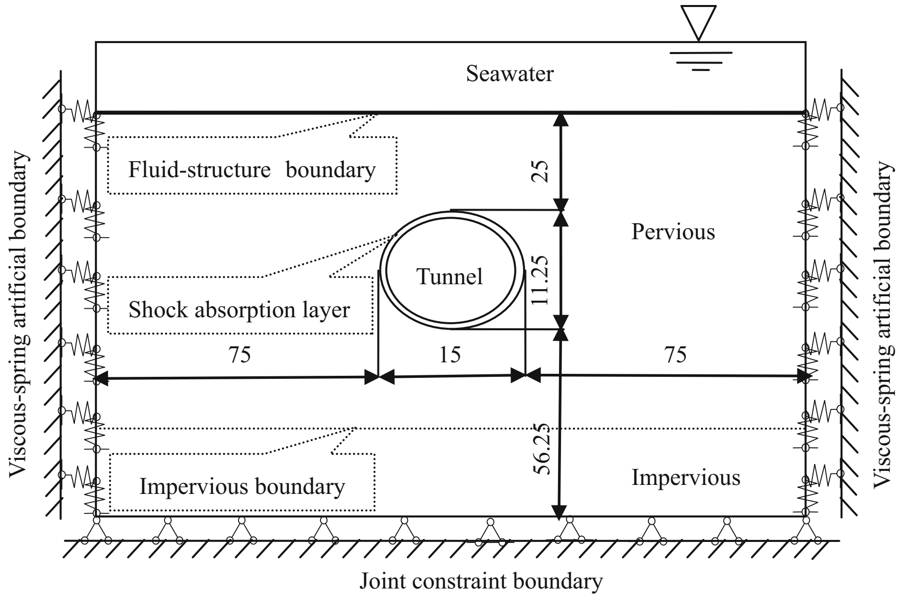

Fig. 1 Schematic of the model (Unit: m)

K_{BT} = 10,121,052 N.s/m, C_{BN} = 3,847,800 N/m, and C_{BT} = 2,056,842 N/m.

The contacts between the tunnel lining and the surrounding rock, primary lining and secondary lining are established by setting the contact friction surface. The friction coefficient of the contact friction surface between the tunnel lining and the rock mass, primary lining or secondary lining should be consistent. In the process of the setting contact surface, the tunnel is considered the target surface (target), and the rock mass surrounding the tunnel is the contact surface (contactor) to permit the convergence of model calculations (Pang 2017).

During earthquake disasters in tunnels, the vault, hance, and inverted arch are the weakest parts of the tunnel. Therefore, the vault (A point), hance (B point), and inverted arch (C point) of the secondary lining of the studied tunnel are selected as the key points in this study (Fig. 2). Unlike the first principal stress–time curve, the peak of first principal stress, and the peak of third principal stress of a lining structure with foam concrete, rubber shock absorption, and a non-damping layer, the damping effect is obtained by setting different levels of shock absorption.

4.2 Calculation Parameters

The Jiaozhou Bay undersea tunnel in Qingdao city is a two-way, six-lane tunnel. The tunnel span is

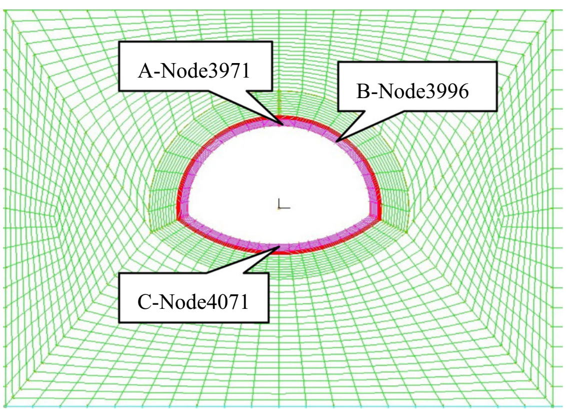

Fig. 2 Key points of the lining structure

approximately 7.8 km, and the subsea length is approximately 3.95 km. It was the second subsea tunnel constructed in China, following the Xiamen Xiang ‘an undersea tunnel.

To improve the simulation of the dynamic response of the rock mass tunnel structure, the Mohr–Coulomb material model is adopted for the rock mass constitutive relationship. The model is based on the perfectly plastic Mohr–Coulomb yield function, a non-associated flow rule, and a tension cutoff. Considering the weak water activity when the seabed depth exceeds a certain value, a permeable layer located 48 m below the interface between the rock mass and seawater is established. In porous media, the remaining portion of the subsurface is considered an impermeable layer. The Mohr–Coulomb material model is chosen as the constitutive equation for lining concrete. The thicknesses of the primary and second linings are 0.3 and 0.5 m, respectively. For seawater, the incompressible constant parametric model is selected, and the FCBI-C element is adopted. A free liquid surface is also defined. The density and default bulk modulus are 10.09 kN/m^3 and 10^{20} Pa, respectively. The thicknesses of the foam concrete and the rubber shock absorption layer are both 0.20 m. According to the actual situation in the Jiaozhou Bay undersea tunnel area in Qingdao city and the existing literature (Cheng et al. 2013, 2016, 2017a, b), the excess pore water pressure due to the seismic impact is not considered in this paper. The parameters are shown in Table 1.

4.3 Seismic Wave

The earthquake disaster examples show that for the seismic response analysis of the tunnel structure, the simulation is more realistic and the results are more reasonable when horizontal and vertical seismic loads are considered.

The El Centro wave, the world's first successful record of the entire seismic process, is of great significance in seismic research. Therefore, the acceleration time history curve of the El Centro earthquake wave in 1940 (north–south; magnitude: M = 6.7; epicentral distance: 9.3 km; maximum acceleration: 2.49 m/s^2) is adopted. According to the existing codes, the peak value is adjusted to 0.2 g, which is equivalent to the eighth-degree fortification criterion. The duration is t_d = 10 s. Figure 3 shows the Y-direction ground motion. The ground motion in the Z-direction is taken as two-thirds that in the Y-direction. To simulate the shear and compression waves, the acceleration time histories in the Y- and Z-directions are based on inputs from the bottom of the limited area.

4.4 Damping Effect Analysis

Different shock absorption materials have different damping effects. Therefore, unlike the first principal stress–time curve, the peak of the first principal stress, and the peak of the third principal stress of the lining structure with foam concrete, rubber shock absorption, and a non-damping layer, the damping effect is derived by setting different shock absorption levels. In this paper, a 2-D solid element is used to simulate the lining. Stress is easier to obtain for solid elements than for axial and flexural elements. Thus, this paper mainly analyzes the stress results.

1. Rubber isolation
   In the case of the bidirectional seismic waves, the time history curves of the first principal stress and the third principal stress in key parts of a secondary lining structure around an undersea tunnel are shown in Figs. 4 and 5 with and without a rubber shock absorption layer. The peaks of the first and third principal stresses are shown in Table 2.
   Figures 4 and 5 and Table 2 show that a rubber isolation layer effectively improves the seismic

Table 1 Calculation parameters of materials

Materials	Elastic modulus *E* (GPa)	Poisson ration μ	Density γ(kN/m^3)	Cohesion *c* (kPa)	Internal friction angle *φ* (°)	Porosity *n*(%)	Permeability *K* (m/s)	Tensile strength σ_t (MPa)	Damping
Pervious rock mass	5	0.3	21.56	600	35	0.2	1.00E−06	1.12	0.065
Impervious rock mass	5	0.3	21.56	600	35	–	–	1.12	0.065
First lining	30	0.167	24.5	3180	54.9	–	–	2.01	0.03
Second lining	30	0.167	24.5	3180	54.9	–	–	2.01	0.03
Foam concrete	0.27	0.21	5.46	50	15	–	–	–	0.04
Rubber	0.0025	0.45	9.8	0.6	6	–	–	–	0.2

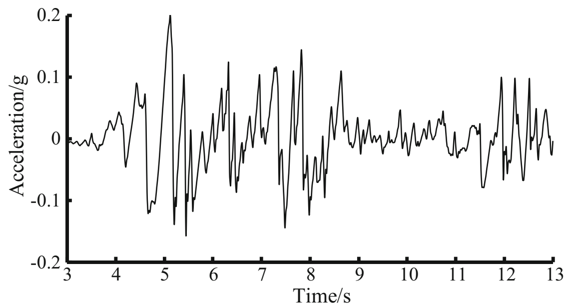

Fig. 3 El-Centro earthquake wave

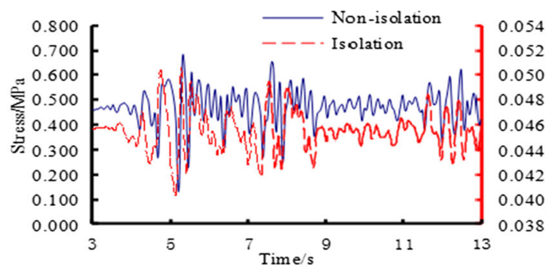

(a) Vault

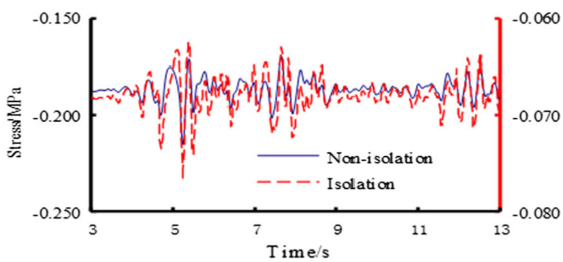

(b) Hance

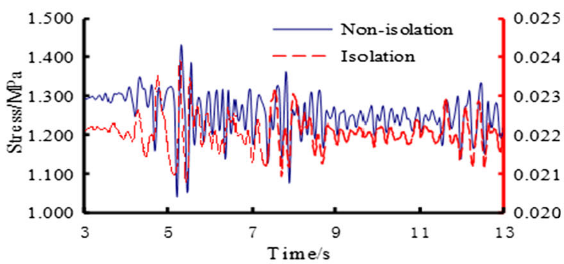

(c) Inverted arch

Fig. 4 Time history curves of the first principal stress

performance of the tunnel structure. Additionally, the mechanical performance of the tunnel lining structure can be significantly improved. The peaks of the first and third principal stresses in key parts of the tunnel structure are reduced to various degrees. A rubber isolation layer cannot change the moment when the peak stress is reached in the lining structure. However, the stress variation is consistent with time, and the time history curve is similar to the curve in the case without isolation. Thus, according to the existing literature (Xu 2014), the rubber isolation layer will not change the spectrum characteristics of the tunnel structure. The rubber isolation layer can only change the principal stress value of the lining structure and cannot change the stress state of the vault and inverted arch. For example, the stress state is a tension state before adding the rubber isolation layer, and the stress state remains a tension state after establishing the rubber isolation layer.

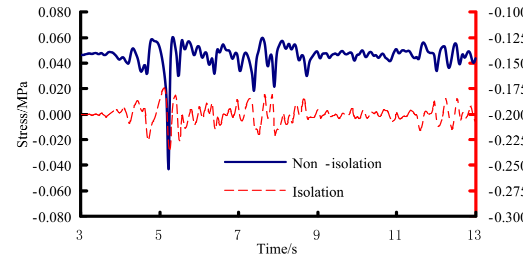

(a) Vault

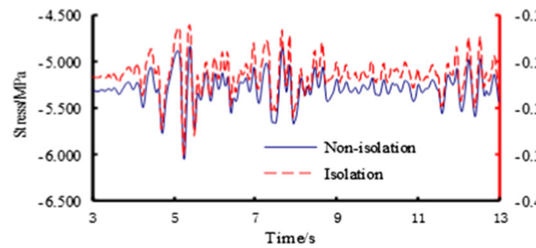

(b) Hance

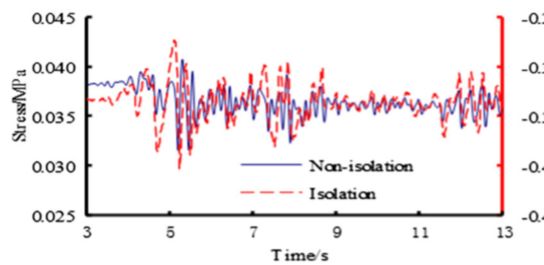

(c) Inverted arch

Fig. 5 Time history curves of the third principal stress

2. Foam concrete isolation layer
   In the case of bidirectional seismic waves, the time history curves of the first principal stress and the third principal stress in the key parts of the secondary lining structure around an undersea tunnel are shown in Figs. 6 and 7 with and without a foam concrete isolation layer. The first and third

Table 2 Comparison of peaks of the first and third principal stress with rubber isolation or not/MPa

Position	A (vault)		B (hance)		C (inverted arch)	
Stress	σ_1^{max}	σ_3^{max}	σ_1^{max}	σ_3^{max}	σ_1^{max}	σ_3^{max}
Non-isolation	0.69	0.06	− 0.22	− 6.05	1.43	0.04
Isolation	0.05	− 0.24	− 0.077	− 0.37	0.024	− 0.4

Positive signs represent tension; negative signs represent compression

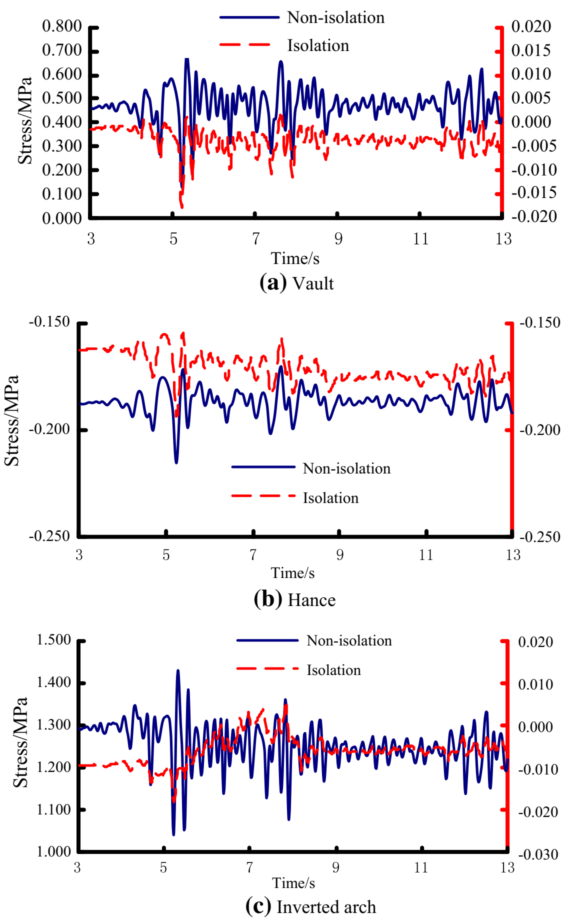

Fig. 6 Time history curves of the first principal stress

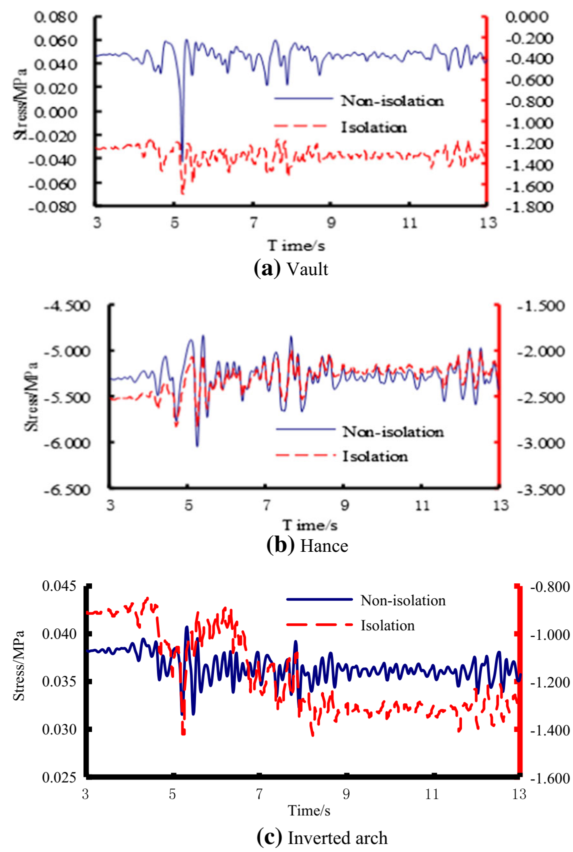

Fig. 7 Time history curves of the third principal stress

principal stress peaks are shown in Table 3. Figures 6 and 7 and Table 3 show that the foam concrete isolation layer not only change the principal stress value of lining structure but also change the stress states of the vault and inverted arch. For example, the stress state is a tension state before establishing the foam concrete isolation layer, and the stress state is compression after establishing the foam isolation layer.

In general, from the perspective of the main stress, establishing the isolation layer can isolate the binding force of the rock mass around the lining structure. Thus, the earthquake damage is reduced and the lining structure is protected.

Because the Mohr–Coulomb model is used for the rock and the concrete lining, it is necessary to study the effects of isolating measures on the shear stress of the subsea tunnel. In the analysis, the maximum shear stress appears in the secondary lining. The calculation results are shown in Table 4.

Table 3 Comparison of the first and third principal stress peaks with foam concrete isolation or not/MPa

Position	A (vault)		B (hance)		C (inverted arch)	
Stress	σ_1^{max}	σ_3^{max}	σ_1^{max}	σ_3^{max}	σ_1^{max}	σ_3^{max}
Non-isolation	0.69	0.06	− 0.22	− 6.05	1.43	0.04
Isolation	0.0015	− 1.69	− 0.194	− 2.83	0.0049	− 1.43

Positive signs represent tension; negative signs represent compression

As shown in Table 4, compared with a non-isolated subsea tunnel, the shear stress of the secondary lining structure of the subsea tunnel is effectively decreased by the two types of isolation measures, and the shear stress decrease caused by rubber isolation layer is significantly greater than caused by the foam isolation layer. Taking effective isolation measures can reduce the probability of shear failure for a lining structure and enhance the safety of subsea tunnels.

4.5 Effect of Shock Absorption Measures on the Dynamic Tunnel Response

To fully consider the dynamic response of a submarine tunnel under earthquake actions after damping measures are adopted, the dynamic responses are studied in cases with no damping, foam concrete damping and rubber damping, and different overlying rock thicknesses and water depths are considered. According to changes in the first and the third principal stresses, the effects of different overlying rock thicknesses and water depths on the dynamic tunnel response can be observed, and the effect on shock absorption after taking these measures can be evaluated.

1. No damping

a. Effect of the overlying rock thickness on the first and the third principal stresses
To obtain the effects of different overlying rock thicknesses on the first and the third principal stresses without isolation measures, the overlying water depth is held constant at 20 m while the thickness of the overlying rock is varied at values such as 25 m, 35 m and 45 m. The first and the third principal stress nephograms are shown in Tables 5 and 6.

b. Effect of seawater depth on the first and the third principal stresses
To obtain the effects of different seawater depths without damping on the first and the third principal stresses, the overlying rock thickness is held constant at 25 m while the seawater depth is varied at 20 m, 30 m and 40 m. The first and the third principal stress nephograms are shown in Tables 7 and 8.

Table 4 Comparison of shear stress calculation results

Type	Non-isolation	Foam concrete isolation	Rubber isolation
Nephogram of shear stress	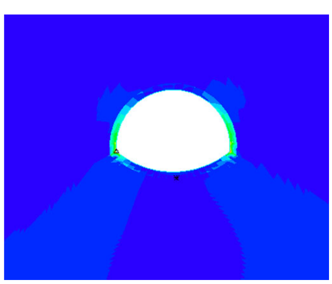	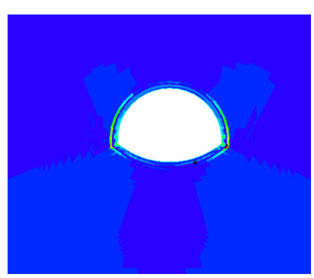	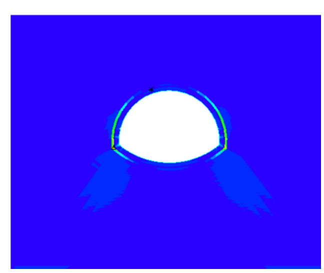
Maximum shear stress (MPa)	5.7346	4.4656	1.9653

Table 5 The first principal stress (σ_1) nephograms under different overlying rock thickness

(1) 25 m

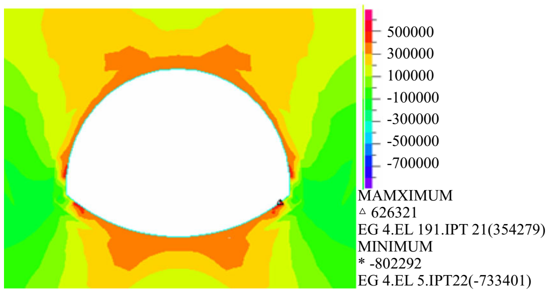

(2) 35 m

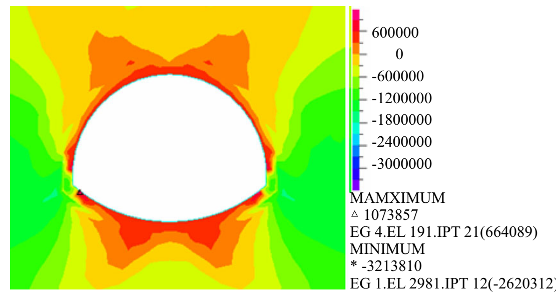

(3) 45 m

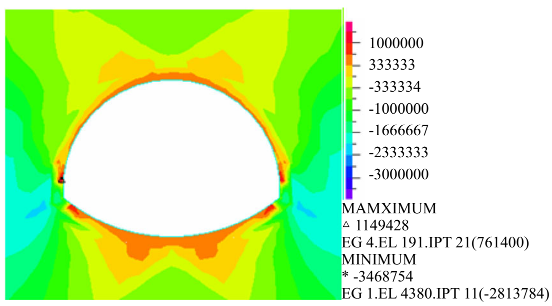

σ_1

Overlying rock thickness/m	Vault $\sigma_{A(MPa)}$	Inverted arch $\sigma_{B(MPa)}$	Arch waist $\sigma_{C(MPa)}$
25	0.405	0.633	− 0.217
35	0.919	0.947	− 0.312
45	0.946	1.022	− 0.350

From Tables 5 and 7, when the water depth is set to 20 m and the thickness of the overlying rock is set to 25 m, 35 m or 45 m, the tensile stresses at the inverted arch and the vault increase with increasing overlying rock thickness. When the overlying rock thickness increases from 25 to 35 m, the tensile stress exhibits considerable mutation. When the overlying rock thickness is 45 m, the tensile stress is close to the ultimate tensile stress of concrete. Thus, attention should be paid to local failure because of tensile stress beyond the stress limit. When the overlying rock thickness is taken as a constant value of 25 m and the overlying water depths are 20 m, 30 m and 40 m, the tensile stresses at the inverted arch and vault slowly change with increasing overlying water depth. The tension zones in the subsea tunnel are generally distributed in the vault and inverted arch; therefore, vaults and inverted arches subjected to earthquake actions will be locally damaged, and some shock absorption measures should be taken.

Tables 6 and 8 show that when the seawater depth is 20 m and the thickness of the overlying rock is 25 m, 35 m or 45 m, the compressive stress of the lining and rock mass surrounding the tunnel increases with increasing overlying rock thickness, and the change is obvious. When the thickness of the overlying rock is constant at 25 m and the overlying water depth is 20 m, 30 m or 40 m, the compressive stress of the lining and rock mass surrounding the tunnel increases with increasing overlying seawater depth. The compression zone is generally distributed in the arch feet and arch waist on both sides of the subsea tunnel. Thus, compression failure must be considered at the arch feet and arch waist.

According to the above calculations under seepage and earthquake actions, the tensile stress is mainly concentrated at the vault and inverted arch, and the compressive stress is concentrated at the arch waist. Therefore, when considering an earthquake, some measures should be taken to strengthen the structure. When the water depth is taken as a constant value, the stress concentration is more obvious as the overburden thickness increases and the security decreases. When the overlying rock thickness is held constant, deeper

Table 6 The third principal stress (σ_3) nephograms under different overlying rock thickness

(1) 25 m

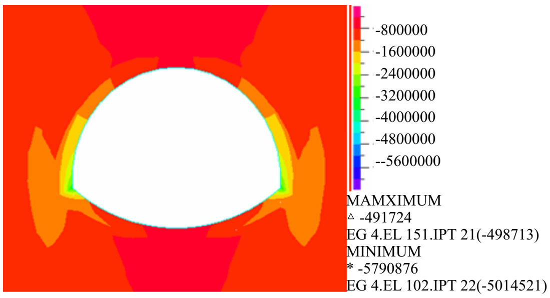

(2) 35 m

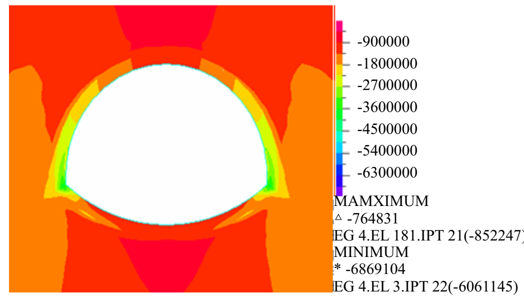

(3) 45 m

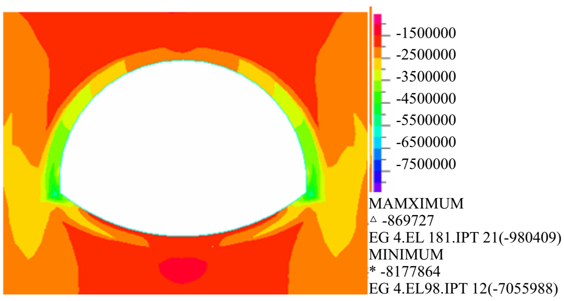

σ_3

Overlying rock thickness/m	Vault σ_A/MPa	Inverted arch σ_B/MPa	Arch waist σ_C/MPa
25	− 0.022	− 0.014	− 5.263
35	− 0.024	− 0.017	− 6.465
45	− 0.028	− 0.021	− 8.038

seawater values increase the stress concentration, but the effect of seawater depth is not as obvious as the effect of the overburden thickness.

2. Foam concrete damping
a. Effect of the overlying rock thickness on the first and the third principal stresses
   To obtain the influence of the overlying rock thickness on the first and the third principal stresses around the subsea tunnel when foam concrete damping is used, the overlying water depth is set to 20 m, and the thickness of the overlying rock is set to 25 m, 35 m and 45 m. The first and the third principal stress nephograms are shown in Tables 9 and 10.
b. Effect of water depth on the first and the third principal stresses
   To obtain the effects of different overlying water depths on the first principal stresses of the tunnel with a damping layer, the overlying rock thickness is set to 25 m, and the overlying water depths are set to 20 m, 30 m and 40 m. The first principal stress nephograms of the tunnel are shown in Tables 11 and 12.

Tables 9 and 11 show that for the undersea tunnel with a shock absorption layer made of foam concrete, the distribution of the tensile zone is mainly concentrated on both sides of the arch feet. When the seawater depth is set to 20 m and the overlying rock thickness is 25 m, 35 m or 45 m, compared with the case of no damping, the tensile stress on the vault and inverted arch slowly changes with increasing thickness of the overlying rock. When the overburden thickness is 25 m and the overlying water depth is 20 m, 30 m or 40 m, the tensile stress on the vault increases with water depth, but the change is relatively stable. However, after using foam concrete, the maximum tensile stresses on the vault and inverted arch are greatly reduced.

As shown in Tables 10 and 12, the compression zone is mainly distributed at the arch feet and the sides of the arch waist after foam concrete damping is established. Thus, compression failure at the arch feet

Table 7 The first principal stress (σ_1) nephograms under different sea water depth

(1) 20 m

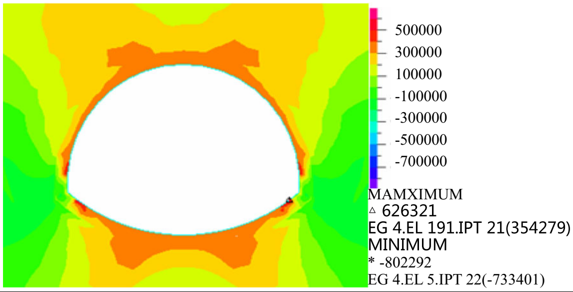

(2) 30 m

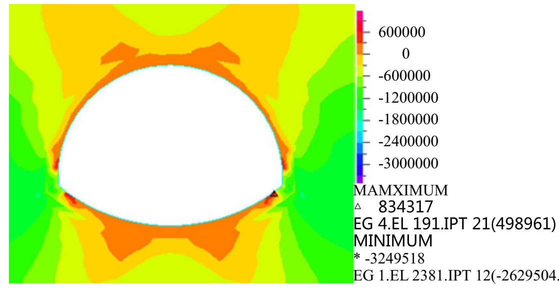

(3) 40 m

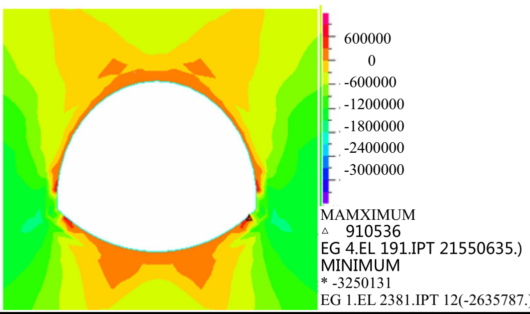

σ_1

Sea water depth /m	Vault σ_A/MPa	Inverted arch σ_B/MPa	Arch waist σ_C/MPa
20	0.073	0.674	− 0.321
30	0.075	0.985	− 0.363
40	0.084	0.982	− 0.401

and arch waist must be considered. Under the condition that the seawater depth is 20 m and the overlying rock thickness is 25 m, 35 m or 45 m, the compression stress increases with increasing overlying rock thickness, and the change is obvious. When the overlying rock thickness is 25 m and the overlying water depth is 20 m, 30 m or 40 m, the compressive stress at the arch waist increases with increasing water depth, but the change is not obvious. Compared with the results without damping, after adding foam concrete, the maximum pressure on the arch waist does not change considerably, but the maximum compressive stress is much smaller than the compressive stress limit of concrete.

3. Rubber shock absorber

a. Effect of the overlying rock thickness on the first and the third principal stresses

   To obtain the influence of the overlying rock thickness on the first and third principal stresses of the tunnel with a damping layer, the overlying water depth is set to 20 m, and the thickness of the overlying rock is set to 25 m, 35 m and 45 m. The first and third principal stress contours are shown in Tables 13 and 14.

b. Effect of water depth on the first and the third principal stresses

   To obtain the influence of the overlying water depth on the first and third principal stresses of the tunnel with a damping layer, the overlying rock thickness set to 25 m, and the overlying water depth is set to 20 m, 30 m and 40 m. The first principal stress nephograms are shown in Tables 15 and 16.

As shown in Tables 13 and 15, for the subsea tunnel with a rubber damping layer, the tensile zone is mainly distributed on both sides of the arch feet. After adding rubber shock absorption, the tensile stress at the vault and the compressive stress at the arch waist still increase with increasing overburden thickness, but compared with the case with no damping, the stress value effectively decreases. Under the condition that the seawater depth is 20 m and the overlying rock

Table 8 The third principal stress (σ_3) nephograms under different sea water depth

(1) 20 m

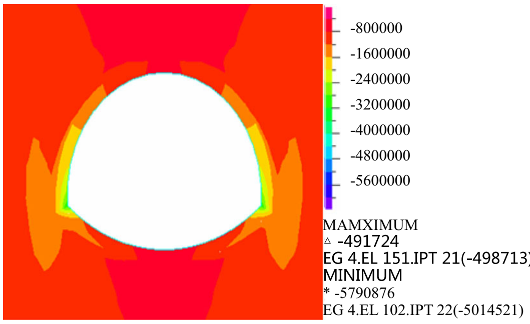

(2) 30 m

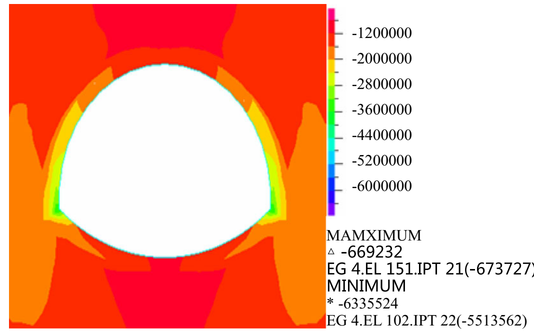

(3) 40 m

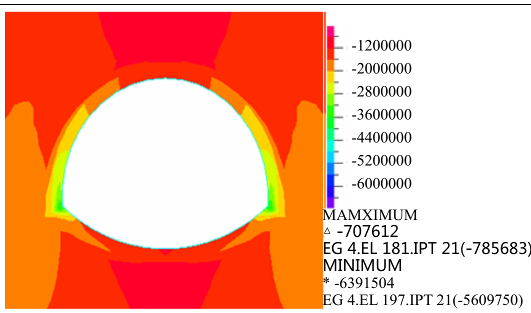

σ_3

Sea water depth/m	Vault	Inverted arch	Arch waist
	σ_A/MPa	σ_B/MPa	σ_C/MPa
20	− 0.0011	− 0.015	− 1.981
30	− 0.0018	− 0.016	− 2.198
40	− 0.0033	− 0.016	− 2.423

thickness is 25 m, 35 m and 45 m, compared with the case with no damping, the tensile stresses at the vault and the inverted arch increase with increasing thickness of the overlying rock, but the change is gradual. When the overburden thickness is 25 m and the overlying water depth is 20 m, 30 m and 40 m, the tensile stress at the vault increases with increasing water depth. However, compared with the case with no isolation layer, the maximum tensile stresses at the vault and the inverted arch are greatly reduced by rubber isolation, and the rubber isolation reduces tensile stress at the vault more so than does foam concrete.

As shown in Tables 14 and 16, for the subsea tunnel with a rubber layer, the compressive zone is mainly distributed at the arch feet and the side arch waist. Thus, compression failure must be considered at the arch feet and arch waist. When the seawater depth is 20 m and the overlying rock thickness is 25 m, 35 m and 45 m, the stress on the lining and rock mass surrounding the tunnel increases with increasing overlying rock thickness, and the change is relatively obvious. When the overburden thickness is 25 m and the overlying water depth is 20 m, 30 m and 40 m, compared with the case with no isolation, the compressive stress at the arch waist minimally changes with increasing water depth after adding rubber isolation, but the maximum compressive stress is still far less than the compressive stress limit of concrete.

As observed from the results with no isolation, foam concrete isolation and rubber isolation at

Table 9 The first principal stress (σ_1) nephograms under different overlying rock thickness

(1) 25 m

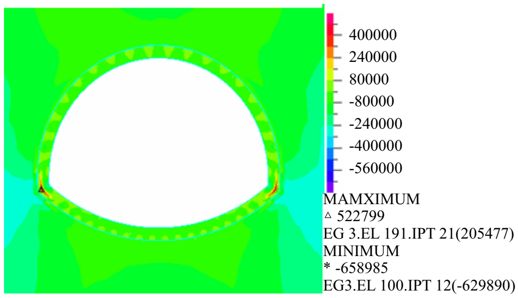

(2) 35 m

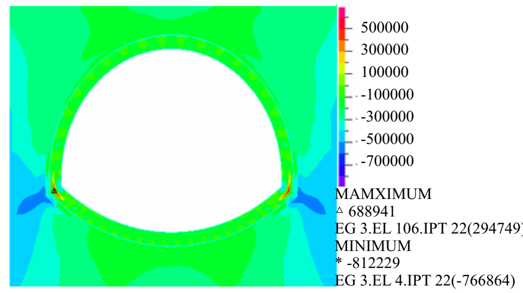

(3) 45 m

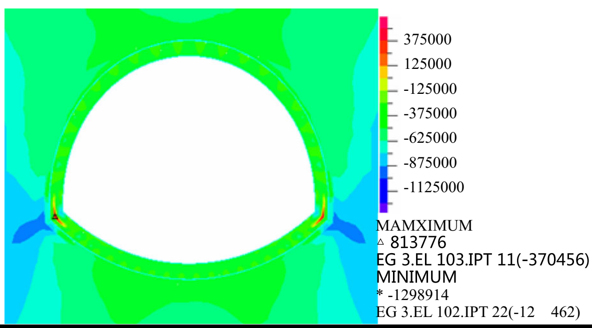

σ_1

Overlying rock thickness/m	Vault σ_A/MPa	Inverted arch σ_B/MPa	Arch waist σ_C/MPa
25	0.179	0.0012	− 0.342
35	0.170	0.0013	− 0.433
45	0.183	0.0096	− 0.529

different rock cover thicknesses and seawater depths, the maximum tensile stress at the arch vault and inverted arch and maximum compressive stress at the arch waist increase with increasing overburden thickness and water depth. After considering isolation, the maximum tensile stress changes in a relatively stable manner with increasing overburden thickness and water depth, but the maximum compressive stress at the arch waist still increases with increasing overburden thickness and water depth. The damping effect of the rubber and foam concrete is roughly the same.

Compared with the case with no isolation, both types of isolation measures can effectively reduce the maximum tensile stress at the vault and inverted arch. When the water depth is constant and the thickness of the overburden increases, the maximum compressive stress at the arch waist can be greatly reduced. Additionally, when the rock cover thickness is constant and the water depth increases, the effect of isolation is not obvious. However, because of the good compressive ability of concrete, the limit of the maximum compressive stress at the arch waist is far less than the compressive stress limit of concrete.

Table 10 The third principal stress (σ_3) nephograms under different overlying rock thickness

(1) 20 m

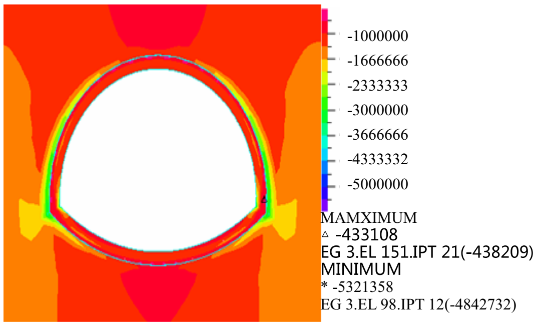

(2) 30 m

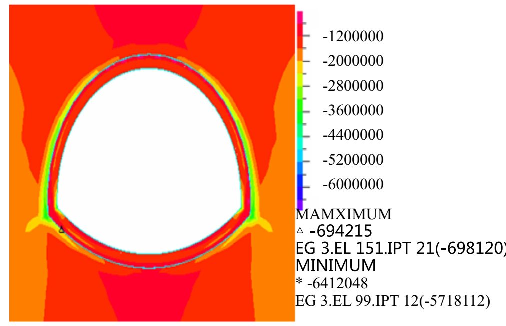

(3) 40 m

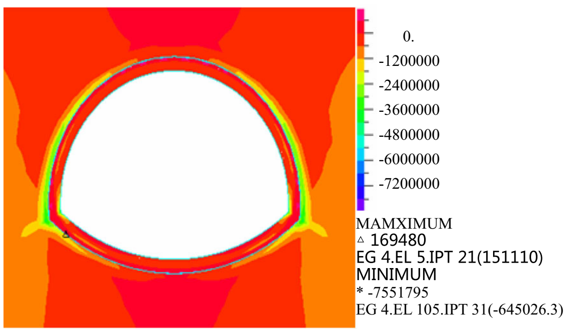

σ_3

Overlying rock thickness/m	Vault σ_A/MPa	Inverted arch σ_B/MPa	Arch waist σ_C/MPa
25	– 0.0011	– 0.066	– 2.061
35	– 0.0051	– 0.066	– 2.762
45	– 0.0256	– 0.066	– 3.284

Therefore, some seismic measures can effectively decrease the maximum tensile stress and achieve the main objectives of many engineering applications.

4.6 Effects of Shock Absorption Measures on Seepage

Seepage is an important feature of subsea tunnels, and it influences tunnel stress and safety. The results of pore water pressure calculations involving the subsea tunnel are shown in Table 17.

Table 11 The first principal stress (σ_1) nephograms under different sea water depth

(1) 20 m

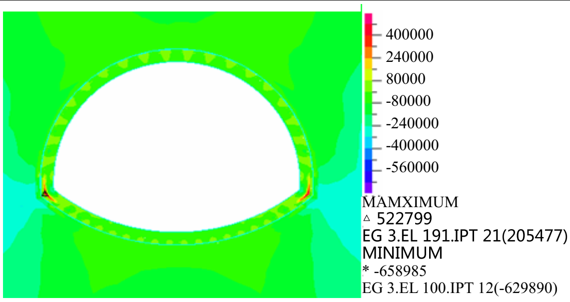

(2) 30 m

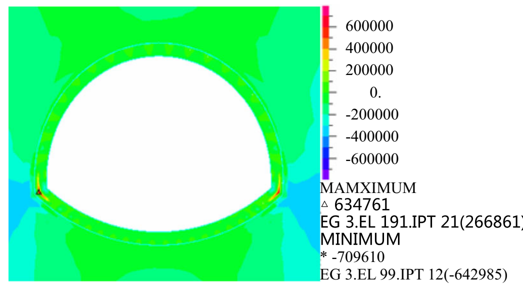

(3) 40 m

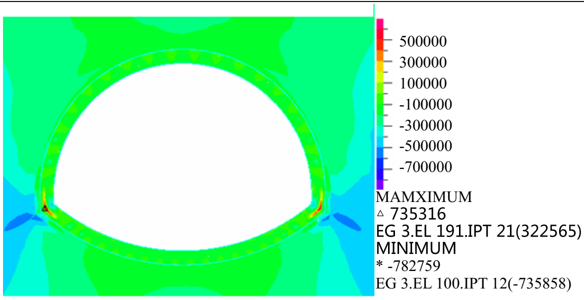

σ_1

Sea water depth /m	Vault σ_A/MPa	Inverted arch σ_B/MPa	Arch waist σ_C/MPa
20	0.058	0.0016	– 0.301
30	0.062	0.0023	– 0.376
40	0.051	0.0017	– 0.411

As shown in Table 17, the pore water pressure of the subsea tunnel under the action of seepage decreases after adopting the isolation measures. This change is likely because of the reflection action of seismic waves in the isolation layer. Additionally, the increase in pore water pressure caused by foam isolation is significantly greater than that caused by rubber isolation.

5 Conclusions

First, establishing an isolation layer cannot fundamentally change the dynamic seismic response value of a tunnel lining structure. Because isolations are associated with buffering and energy dissipation, the stress transfer coefficient decreases, which improves the vibrational isolation effects on lining structures.

Table 12 The third principal stress (σ_3) nephograms under different sea water depth

(1) 20 m

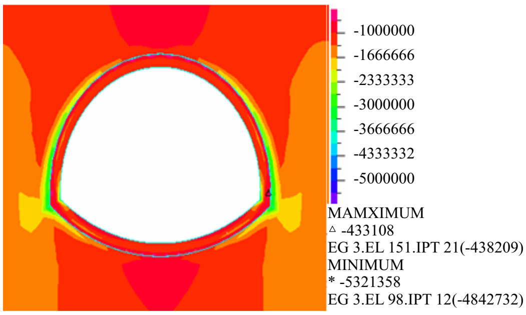

(2) 30 m

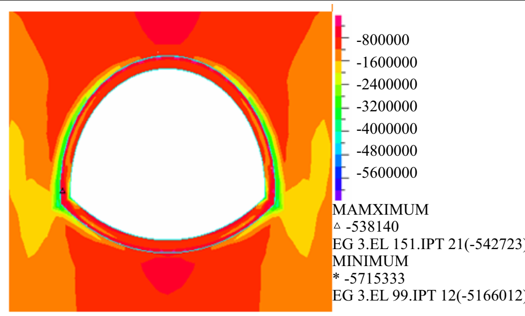

(3) 40 m

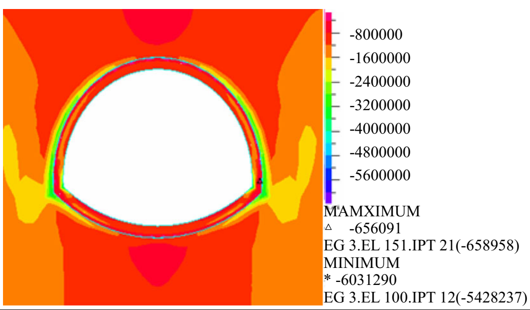

σ_3

Sea water depth/m	Vault σ_A/MPa	Inverted arch σ_B/MPa	Arch waist σ_C/MPa
20	– 0.0015	– 0.069	– 1.893
30	– 0.0021	– 0.071	– 2.271
40	– 0.0037	– 0.080	– 2.487

Second, compared with the rubber layer, the foam concrete isolation layer may change the force direction at the vault and inverted arch in the secondary lining structure, namely, from a very unfavorable tension state to a compression state, which improves the isolation effect.

Third, although the foam concrete and rubber have certain isolation effects, considering significant seawater seepage and extremely strong seawater corrosion, the lifespan of rubber will be greatly reduced. Additionally, the rubber layer easily ages and gradually loses its original seismic performance at relatively

Table 13 The first principal stress (σ_1) nephograms under different overlying rock thickness

(1) 25 m

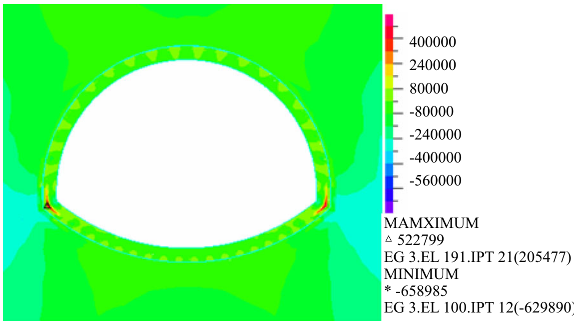

(2) 35 m

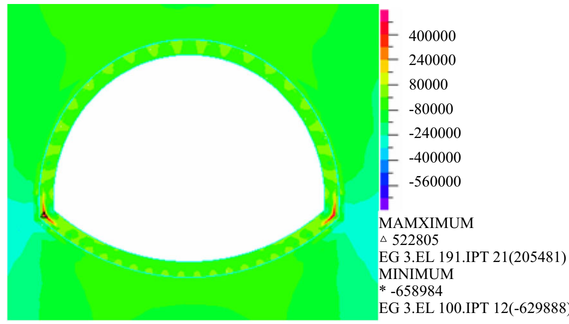

(3) 45 m

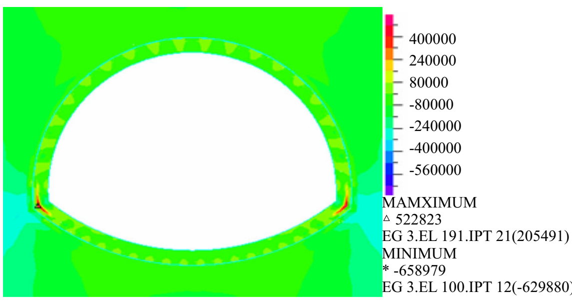

σ_1

Overlying rock thickness/m	Vault σ_A/MPa	Inverted arch σ_B/MPa	Arch wais σ_C/MPa
25	0.128	0.0019	– 0.321
35	0.131	0.0025	– 0.383
45	0.139	0.0031	– 0.479

high stress states; therefore, we suggest that foam concrete isolation be used.

Fourth, when implementing isolation measures, the thicker the overlying rock is, the higher the stress concentration in the subsea tunnel will be. By contrast, the effect of water depth on the tunnel stress is relatively small. For different thicknesses of overlying rock and different water depths, isolation measures can effectively reduce the tensile stress at the vault and inverted arch and offset the relatively low tensile strength of concrete. Overall, the stress concentration

Table 14 The third principal stress (σ_3) nephograms under different overlying rock thickness

(1) 20 m

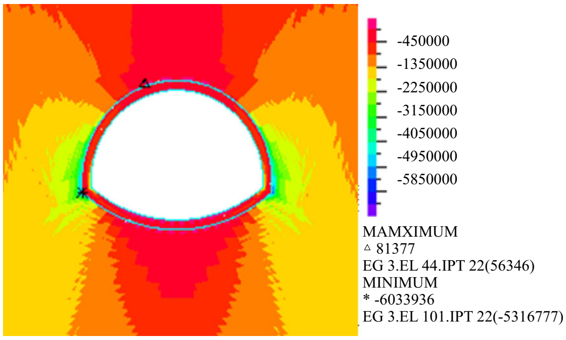

(2) 30 m

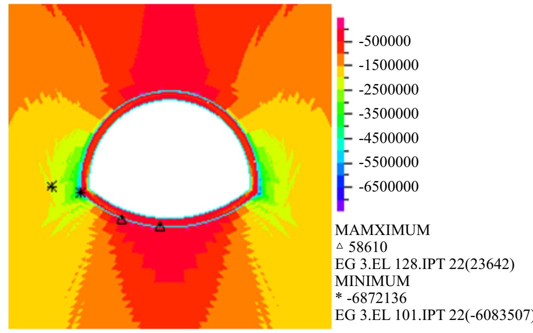

(3) 40 m

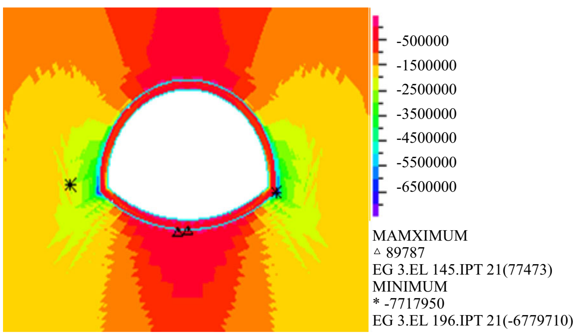

σ_3

Overlying rock thickness/m	Vault σ_A/MPa	Inverted arch σ_B/MPa	Arch waist σ_C/MPa
25	− 0.0021	− 0.053	− 1.985
35	− 0.0025	− 0.061	− 2.526
45	− 0.0047	− 0.072	− 3.024

in the tunnel is significantly reduced because of isolation.

Finally, the presented results are for the lightly weathered rock mass surrounding subsea tunnels. For heavily weathered rock masses and broken rock masses, the analysis should be re-designed to include the influence of the surrounding fluid and other factors.

Table 15 The first principal stress (σ_1) nephograms under different sea water depth

(1) 20 m

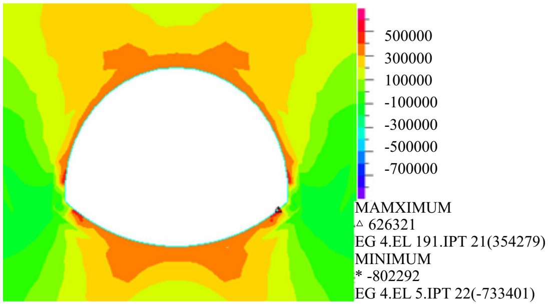

(2) 30 m

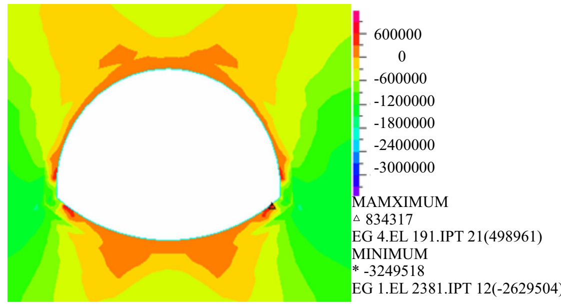

(3) 40 m

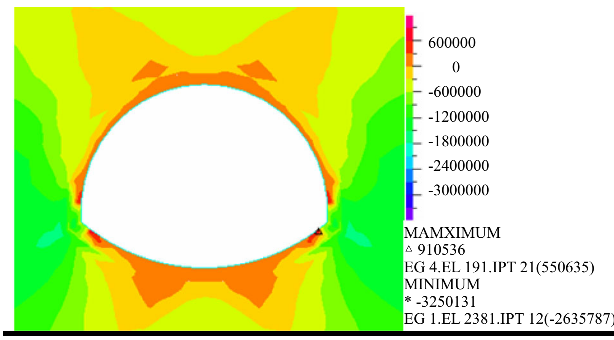

σ_1

Sea water depth /m	Vault σ_A/MPa	Inverted arch σ_B/MPa	Arch waist σ_C/MPa
20	0.047	0.0016	– 0.283
30	0.053	0.0019	– 0.336
40	0.049	0.0017	– 0.402

Table 16 The third principal stress (σ_3) nephograms under different sea water depth

(1) 20 m

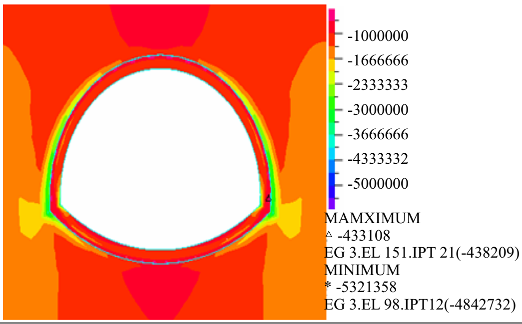

(2) 30 m

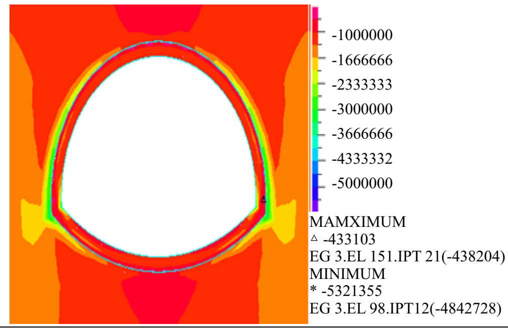

(3) 40 m

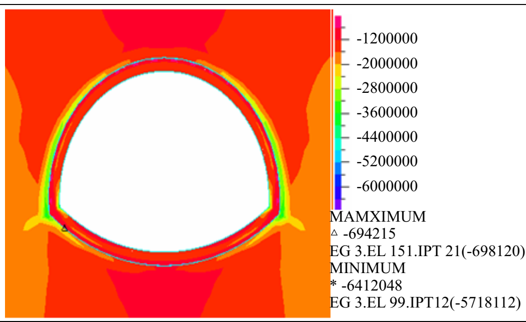

σ_3

Sea water depth/m	Vault $\sigma_{A(MPa)}$	Inverted arch $\sigma_{B(MPa)}$	Arch waist $\sigma_{C(MPa)}$
20	– 0.0016	– 0.054	– 2.067
30	– 0.0023	– 0.062	– 2.358
40	– 0.0027	– 0.073	– 2.516

Table 17 Effect of isolation on pore water pressure

Type	Non-isolation	Foam concrete isolation	Rubber isolation
Nephogram of pore water pressure	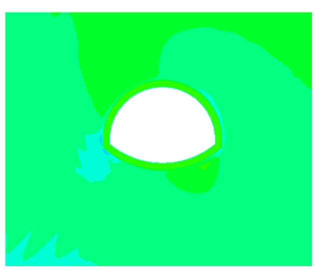		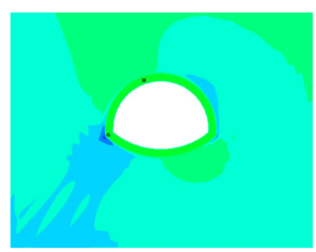
Maximum pore water pressure (MPa)	0.5157	1.0887	0.5158

Acknowledgements This paper is a part of the national natural science foundation of China (Grant Number: 51478212), and a part of the national key basic research and development plan of China (973 plan; Grant Number: 2011CB013600), and a part of the education ministry doctoral tutor foundation of China (Grant Number: 20136201110003).

Compliance with Ethical Standards

Conflict of interests The authors declare that there is no conflict of interests regarding the publication of this paper.

References

Cheng XS, Wang JH, Du XL (2013) Fluid-solid coupling based seismic response analysis of subsea tunnels during seepage. Mod Tunn Technol 50(6):44–51

Cheng XS, Ren Y, Du XL, Zhang YD (2014a) Seismic stability of subsea tunnels subjected to seepage. Sci World J 2014:631925. https://doi.org/10.1155/2014/631925

Cheng XS, Xu WW, Yue CQ, Du XL (2014b) Seismic response of fluid-structure interaction of undersea tunnel during bidirectional earthquake. Ocean Eng 75(1):64–70. https://doi.org/10.1016/j.oceaneng.2013.11.017

Cheng XS, Yu DJ, Liu B et al (2016) Stability analysis of cross sea tunnel with shock absorption subjected to seepage and bi-directional earthquake. J Railw Sci Eng 13(5):882–890

Cheng XS, Li D, Ren Y, Du XL (2017a) Seismic stability analysis of subsea tunnels under the effects of seepage and temperature. Mar Georesour Geotechnol 35(6):806–816

Cheng XS, Zhang XY, Chen WJ et al (2017b) Stability analysis of a cross-sea tunnel structure under seepage and a bidirectional earthquake. Int J Geomech 17(9):06017008. https://doi.org/10.1061/(asce)gm.1943-5622.0000937

Cheng XS, Li GL, Chen J et al (2018) Seismic response of a submarine tunnel under the action of a sea wave. Marine structures 60(2018):122–135. https://doi.org/10.1016/j.marstruc.2018.03.004

Gao WL (2001) Study on seismic responses and vibration-absorption measures for extra-long tunnel of the shallow section in high intensity earthquake zone. Ph.D. thesis of Beijing Jiaotong University

Gao L, Chen YH (2008) Analysis of shock absorption measures in tunnels based on ANSYS software. J Shihezi Univ Nat Sci Ed 26(4):495–498. https://doi.org/10.3969/j.issn.1007-7383.2008.04.025

Gao F, Shi YC, Yan SH et al (2005) Study of two shock absorption measures in tunnel. Chin J Rock Mech Eng 24(2):222–229. https://doi.org/10.3321/j.issn:1000-6915.2005.02.007

Hasheminejad SM, Miri AK (2008) Seismic isolation effect of lined circular tunnels with damping treatments. Earthq Eng Eng Vib 7(3):305–319. https://doi.org/10.1007/s11803-008-0842-7

Huang S, Chen WZ, Yang JP et al (2009) Research on earthquake-induced dynamic responses and aseismic measures for underground engineering. Chin J Rock Mech Eng 28(3):483–490. https://doi.org/10.3321/j.issn:1000-6915.2009.03.006

Kim DS, Konagai K (2000) Seismic isolation effect of a tunnel covered with coating material. Tunn Undergr Space Technol 15(4):437–443. https://doi.org/10.1016/s0886-7798(01)00012-8

Konagai KZ, Kim DS (2001) Simple evaluation of the effect of seismic isolation by covering a tunnel with a thin flexible material. Soil Dyn Earthq Eng 21(4):287–295. https://doi.org/10.1016/s0267-7261(01)00012-4

Li YS (2006) Study on earthquake responses and vibration-absorption measures for mountain tunnel. Ph.D. thesis of Tongji University

Ling YT, Gao B (2008) Study on shock absorption measures for double-lane highway tunnels in high earthquake intensity regions. Tunn Constr 28(4):412–415

Liu JY, Chen GY, Jiang W (2010) Study on shock absorption measures of water-conveyance tunnel. J Disaster Prev Mitig Eng 30(2):196–201. https://doi.org/10.3969/j.issn.1672-2132.2010.02.014

Pang C (2017) Study on the dynamic model of soil-pipe-water interaction for buried pipelines under earthquake. Master degree thesis of Southwest Jiaotong University 17

Shimamura SD, Kasai H, Haruumi M (1999) Seismic isolation effect for a tunnel with a soft isolation layer. Earthq Eng 16(2):143–154

Sun TC (2009). Study on earthquake responses and vibration-absorption measures for two-tunnels of mountain tunnel with staggered space. Ph.D. thesis of Southwest Jiaotong University

Tao JH (2005) Numerical simulation of water waves. Tianjin University Press, Tianjin

Wang ZS (2008) Study on seismic dynamic responses and vibration-absorption measures for portal of double-arch tunnel. Ph.D. thesis of Southwest Jiaotong University

Wang MN, Cui GY (2010) Establishment of tunnel damping model and research on damping effect with model test in highly seismic area. Rock Soil Mech 31(6):1884–1890

Wang X, Dong J (2003) Formulation and study of thermal-mechanical coupling of saturated porous media. Int J Comput Struct 81(8–11):1019–1029. https://doi.org/10.1016/s0045-7949(02)00476-5

Wang ZJ, Gao B, Guan BS (1996) Research of isolation of rock-liner structure systems. J Southwest Jiaotong Univ 31(6):590–594

Xie KH, Zhou J (2002) The finite element analysis theory and application in geotechnical engineering. Science Press, Beijing

Xiong LX, Li TB, Yang LD (2007) Numerical analysis of two-shock absorption measures of tunnel. Hydrogeol Eng Geol 34(4):36–40. https://doi.org/10.3969/j.issn.1000-3665.2007.04.010

Xu TN (2014) Study on nonlinear spectrum of isolated structure and its input energy. Master degree thesis of Lanzhou University of Technology

Yuan S (2008) Seismic response analysis and vibration absorption measure of shallow-depth tunnel. Thesis of Wuhan University of Technology